DOI: 10.26599/FSHW.2026.9251296

Contents lists available at SciOpen

Food Science and Human Wellness

journal homepage: https://www.sciopen.com/journal/2097-0765

China Food Publishing Co.

Glycogen Architecture Dysregulation in Metabolic Dysfunction-Associated Steatohepatitis (MASH): A Therapeutic Avenue via Glycogen Homeostasis

Ziyi Wang [a,b,c,d#], Shasha He [e#], Bi Fang[f#], Renjie Feng [a], Wenshao Li [g], Liang Wang [h,i], Chaoxin Man [j], Huifan Yu [c], Fei Li [c], Mitchell A. Sullivan [k], Na Wang [l,*], Robert G. Gilbert [m,*], Peng Cao [a,b,c,n,o*]

[a] *Department of Pharmacy, Union Hospital, Tongji Medical College, Huazhong University of Science and Technology,Wuhan, Hubei 430074, China*

[b] *Department of Pharmacology, Toxicology and Therapeutics, University of Kansas Medical Center, Kansas City,Kansas 66160, USA*

[c] *Hubei Key Laboratory of Wudang Local Chinese Medicine Research, School of Pharmaceutical Sciences, Hubei University of Medicine, Shiyan, China*

[d] *Centre for Nutrition and Food Sciences, Queensland Alliance for Agriculture and Food Innovation, The Universityof Queensland, Brisbane, Queensland 4072, Australia*

[e] *Beijing Hospital of Traditional Chinese Medicine, Capital Medical University, Beijing, China*

[f] *Department of Gastroenterology，The Third Affiliated Hospital of Soochow University，Changzhou, Jiangsu, 213000,China*

[g] *College of Medicine and Public Health, Flinders University, Sturt Road, Bedford Park, SA 5042, Australia*

[h] *Laboratory Medicine, Guangdong Provincial People's Hospital (Guangdong Academy of Medical Sciences), Southern Medical University, Guangzhou, Guangdong 510080, China.*

[i] *School of Medical and Health Sciences, Edith Cowan University, Joondalup, WA 6027, Australia.*

[j] *Key Laboratory of Dairy Science, Ministry of Education, College of Food Science and Engineering, Northeast Agricultural University, Harbin, 150030, China*

[k] *Centre for Bioinnovation and School of Health, University of the Sunshine Coast, Sippy Downs, Queensland,Australia*

[l] *Department of Pharmacy, Renmin Hospital, Wuhan University, No.99, Zhangzhidong Road, 430060, Wuhan, China*

[m] *Key Laboratory of Plant Functional Genomics of the Ministry of Education/ Jiangsu Key Laboratory of Crop Genomics and Molecular Breeding, College of Agriculture, Yangzhou University, Yangzhou 225009, China; and Co- Innovation Center for Modern Production Technology of Grain Crops, Yangzhou University, Yangzhou 225009,China*

[n] *Hubei Jiangxia Laboratory, Wuhan, China*

ABSTRACT: Metabolic dysfunction-associated steatohepatitis (MASH) is the inflammatory phase of the metabolic dysfunction-associated steatotic liver disease (MASLD) spectrum, and can progress to fibrosis and even carcinoma; currently, there are few effective therapies. The complex branched glucose polymer glycogen is found in significant quantities in the liver; it comprises "β particles", ~20 nm in size, bound as aggregate "α particles", up to hundreds of nm in size. The role of liver glycogen in MASLD and MASH is unknown. Size-exclusion chromatography, fluorophore-assisted carbohydrate electrophoresis and transmission electron microscopy show that, compared with healthy controls, MASLD livers exhibited a higher β-particle content (32.6% vs 40.7%, P <0.05) and a 5 % longer average chain length (ACL); MASH amplified these defects: β-particle fraction rose to 46.1% (P <0.001 vs. control) and ACL to 26 % (P <0.0001 vs. control), indicating this is an early, shared disruption in different stages of MASLD.

[#]Co first authors
***Corresponding author**
wangna_rm@163.com (Na Wang). b.gilbert@yzu.edu.cn (R.G. Gilbert).caopeng1989@hust.edu.cn (Peng Cao).

Received 30 January 2026
Received in revised from 10 March 2026
Accepted 11 May 2026

The glycogen-related proteins (AGL, GBE, GYS, PYGL and PPP1R3B) exhibit opposite trajectories in MASLD and MASH. Therapeutic dietary polyphenols, despite disparate effects on individual glycogen-related enzymes, all reversed aberrant glycogen architecture by increasing α-particle proportions and decreasing chain lengths. Our findings offer a mechanistic blueprint whereby glycogen structure characterization might guide clinical therapeutic strategy.

Keywords: Glycogen, MASH, MASLD, polyphenols

1. Introduction

Metabolic dysfunction-associated steatotic liver disease (MASLD) has emerged as the most prevalent chronic liver disorder worldwide, currently affecting approximately 32% to 34% of the global adult population [1, 2]. As the hepatic manifestation of metabolic syndrome, MASLD encompasses a histopathological spectrum starting from simple steatosis, with about 20% to 30% of cases progressing to metabolic dysfunction-associated steatohepatitis (MASH) [1, 2]. MASH is characterized by the critical presence of hepatocyte ballooning and lobular inflammation, which serve as the primary drivers of progressive fibrosis. Without timely intervention, the condition can advance to cirrhosis, liver failure, and hepatocellular carcinoma (HCC). Notably, MASH has become one of the fastest-growing causes of primary liver cancer mortality globally, with annual HCC-related deaths projected to continue rising due to the dual epidemics of obesity and type 2 diabetes.

Despite this rapidly-growing problem, only two therapeutic agents, resmetirom (Rezdiffra) and, recently, semaglutide, have received accelerated FDA approval for adults with MASH; however, their clinical utilities are limited [3]. In clinical trials, resmetirom achieved outright resolution of steatohepatitis in only 25-30 % of treated subjects, while ≥70 % of patients failed to meet either histological endpoint (MASH resolution with no worsening of fibrosis, or an improvement in fibrosis by at least one stage with no worsening of the MASLD activity score) [4]. Moreover, gastrointestinal adverse events and pruritus (itching) were common side effects, leading to discontinuation in roughly one-sixth of recipients. Semaglutide can cause gastrointestinal side effects such as nausea and vomiting, which also can lead to discontinuation of treatment in some patients. These shortcomings underscore the need for alternative therapeutic strategies that can deliver broader efficacy with an improved safety profile.

A growing body of evidence shows that hepatic glycogen is not merely a passive glucose reservoir, but a dynamic macromolecule whose architecture influences metabolic flux. It is a highly-branched glucose polymer that acts as a blood-glucose reservoir, and accounts for 4-5% of liver weight (the amount, size and number depending on the time in the diurnal cycle). Glycogen molecules are composite particles made up of linked β particles (~20 nm in diameter) [5]. In healthy liver, ~20-nm β-particles are joined together to form α particles, which are up to 300 nm in diameter; the α/β ratio influences glycogen turnover rates, while the underlying chain-length distribution (CLD) is critical for maintaining proper architecture similar to that observed in healthy liver [6, 7]. We have demonstrated that glycogen structure in diabetic subjects is different from that in healthy subjects, shifting toward smaller β-particles and longer chains; this may reduce its ability to buffer blood glucose fluctuations [8, 9]. However, the precise alterations in glycogen

macromolecular structure (CLD and α/*β*-particle composition) across the MASLD-MASH spectrum, and their potential as a therapeutic target, remain unexplored.

Glycogen homeostasis is orchestrated by a tightly regulated enzymatic network. PYGL (glycogen phosphorylase) initiates glycogenolysis by cleaving (1→4)-α glycosidic linkages to release glucose-1-phosphate, whereas AGL (amylo-(1→6)-α-glucosidase) debranches limit-dextrin side chains, ensuring complete glycogen breakdown [10]. GBE1 (glycogen branching enzyme 1) introduces (1→6)-α branches during glycogen synthesis, dictating glycogen particle size and solubility [11]. GYS (the liver isoform of glycogen synthase) catalyzes the rate-limiting step of glycogenesis, and its activity is antagonized by PYGL in a reciprocal fashion [12]. PPP1R3B (protein phosphatase 1 regulatory subunit 3B) serves as a molecular scaffold that targets protein phosphatase 1 to glycogen particles, thereby dephosphorylating and activating GYS while simultaneously inhibiting PYGL, and thus integrating hormonal signals with glycogen storage and release [13, 14]. Collectively, alterations in the abundance or activity of these proteins can cause glycogen architecture dysregulation.

MASLD and MASH has been associated with dysregulated glycogen turnover and impaired glucose homeostasis [15, 16], we therefore hypothesized that the disease would be characterized by a distinct glycogen structural signature, and that interventions aimed at restoring glycogen homeostasis might simultaneously normalize glucose homeostasis and attenuate inflammation progression. By integrating glycogen structural profiling with quantitative assessment of key glycogen-metabolic proteins, we reposition hepatic glycogen from a passive energy store to a dynamic, targetable node that links metabolic flux to MASH resolution. This provides a potential mechanistic blueprint for novel therapies targeting glycogen homeostasis in metabolic liver disease.

2. Methods

2.1 Animal experiments

Male C57BL/6J mice (weights 18-22 g, SYXK 2021-0025) were bought from Hubei Provincial Center for Disease Control and housed under identical environmental conditions with standardized diet composition and feeding protocols in an SPF-class room (25 ℃, light/dark cycle every 12 h). The animal study was reviewed and approved by the Institutional Animal Care and Use Committee of Tongji Medical College, Huazhong University of Science and Technology. The animal care and experimental procedures were carried out in accordance with the Guidelines of the Institutional Animal Care and Use Committee of Tongji Medical College and the National Institutes of Health Guide for the Care and Use of Laboratory Animals. The animal ethics approval number in this study is HUST-IACUC-2025-0060.

A mouse model of MASLD was generated by a long-term administration of a high-fat diet (HFD; D12492, Research Diets, New Brunswick, NJ, USA), which provided 60% of total calories from fat (primarily lard and soybean oil), 20% from protein, and 20% from carbohydrates, with a total energy density of 5.24 kcal/g for 12 weeks, while control mice received an isocaloric matched standard chow in parallel. A mouse model of MASH was induced by 6-week feeding of a MCD diet (Jiangsu Xietong Pharmaceutical

Bio-engineering Co., Ltd., Nanjing, China) to induce the MASH phenotype. The MCD diet provided a caloric density of 4.2 kcal/g, consisting of 16.2% protein (L-amino acid mix), 10.0% fat, and 66.2% carbohydrate (primarily sucrose), with the explicit absence of L-methionine and choline bitartrate. For drug intervention, three polyphenols, namely quercetin (QR), naringenin (NAG) and luteolin (LTL), which have been demonstrated to prevent MASH [17-19], were employed in the present study. All mice were acclimated for one week, then randomly divided into the following five groups (n = 6-10 mice per group), and housed for six weeks: (1) CG group: mice were fed an AIN93G diet (which is isocaloric with an MCD diet); (2) MASH group: mice were fed an MCD diet ; (3) QR group: mice were fed a customized MCD diet, namely an MCD diet with the addition of quercetin (0.05%, w/w); (4) NAG group: mice were fed a customized MCD diet containing naringenin (0.05%, w/w); (5) LTL group: mice were fed a customized MCD diet containing luteolin (0.05%, w/w).

At the end of the animal experiments, a blood sample from each mouse was taken from the orbital sinus. The samples were left at room temperature for at least 30 min before being centrifuged at 3000 × *g* for 10 min to separate the serum. Thereafter, the mice were euthanized by cervical dislocation, and their liver tissues were collected. One portion of the fresh liver tissue was used for hematoxylin eosin (H&E), Oil Red O (ORO), Periodic Acid-Schiff (PAS) and immunohistological staining of GRP78 and p-AMPK protein. The remaining portion of liver was used for glycogen analysis. The serum or hepatic levels of alanine aminotransferase (ALT), aspartate transaminase (AST), total cholesterol (TC) and triglyceride (TG), malondialdehyde (MDA) and glutathione (GSH) were determined using commercial kits (Beijing Solarbio Science & Technology Co., Ltd.). Fasting blood glucose (FBG) was measured from blood obtained from the tail vein of mice fasted overnight, and the concentration of glucose measured using a one-touch glucometer (Bayer, Leverkusen, Germany).

2.2 Glycogen extraction

Liver extraction was performed using an optimized sucrose density gradient centrifugation method [9]. Three mL of glycogen isolation buffer (50 mmol/L Tris, pH 8, 150 mmol/L NaCl, 2 mmol/L EDTA, 50 mmol/L NaF, and 5 mmol/L sodium pyrophosphate) were added to a 10-mL tube, to which frozen mouse-liver tissue (~500 mg) was then added. Each sample was homogenized using a tissue homogenizer (IKA T25, Staufen, Germany) on ice, then 100 μL was removed for glycogen content determination (method described in section 2.3). All samples were centrifuged at 6000 × *g* for 10 min at 4 ℃. The remaining supernatant of each sample was transferred to Beckman ultracentrifuge tubes (10.4 mL, Centrifuge Bottles Polycarbonate, 16 mm × 76 mm), and then centrifuged at 3.6×10^5 *g* for 1 h 30 min at 4 ℃. After discarding the remaining supernatants, the resulting pellets were resuspended in 2 mL of glycogen isolation buffer. All samples were layered over a 10 mL stepwise sucrose gradient (4 mL 37.5% sucrose in glycogen isolation buffer, 4 mL 75% sucrose in glycogen isolation buffer) in 10.4 mL ultracentrifuge tubes, and then samples were centrifuged at 3.6×10^5 *g* for 2 h at 4 ℃. After discarding the supernatants, the resulting pellets were resuspended in 400 μL of deionized water. 1600 μL of ethanol was added to precipitate glycogen, with

samples being stored at -30 ℃ for at least 1 h to aid precipitation. Samples were centrifuged at 6000 × *g* for 10 min at 4 ℃, the supernatants then discarded, and the pellets resuspended in 200 μL of deionized water. This ethanol precipitation process was repeated 3 times, with the final glycogen pellet being re-dissolved in 200 μL of deionized water. These samples were frozen and freeze-dried overnight.

2.3 Glycogen content analysis

The liver-glycogen content was analyzed by the amyloglucosidase oxidase/peroxidase (GOPOD) method. 8 μL of solution from the homogenate of the glycogen extraction process described above, 5 μL of amyloglucosidase (AMG) (3260 U/mL, tested with a Megazyme kit [Bray, Co. Wicklow, Ireland] using soluble starch), and 100 μL of sodium acetate buffer (1 M, pH 4.5) was made up to 500 μL with deionized water. Controls using deionized water instead of AMG were used to determine the background glucose levels. Samples were incubated at 50 ℃ for 30 min, while controls were kept cold. All samples and controls were centrifuged at 6 000 × *g* for 10 min, then 300 μL of resulting supernatant was added to 1 mL of GOPOD reagent (Megazyme). Standards containing 0, 10, 20, 30, 40 and 50 μg of D-glucose were added to 1 mL GOPOD to obtain a calibration curve. All samples were then incubated at 50 ℃ for 30 min. A UV-vis spectrophotometer was used to analyze the absorbance of each sample at 510 nm. The glycogen content was calculated based on the D-glucose standard curve and involved subtracting those of the control samples (with no AMG) from the experimental ones.

2.4 Chain length distributions

The CLD is the relative number or weight of chains as a function of the degree of polymerization of that chain. This was obtained by fluorophore-assisted carbohydrate electrophoresis (FACE) [20]; this technique cannot go above degree of polymerization ~150, but this covers the entire range of interest here [21]. Firstly, 0.5 mg of dry glycogen from the last step of glycogen extraction was transferred to 1.5 mL tubes, then 90 μL of deionized water with 1.5 μL of sodium azide (0.04 g/mL) was added. Then, 5 μL of acetic acid buffer (0.1 M, pH 3.5) and 2 μL of debranching enzyme (isoamylase) solution (Megazyme, 180 U/mg) was added to cleave (1→6)-α linkages of the glycogen, then the solution was incubated at 37 ℃ for 3 h. 5 μL of sodium hydroxide solution (0.1 M) was added, which neutralized the mixture to pH 7. The solution was kept at 80 ℃ for 1 h, then frozen in liquid nitrogen and freeze-dried overnight. The solution of debranched glycogen chains was labeled with 1.5 μL of 8-aminopyrene-1,3,6-trisulfonate (APTS) solution (0.2 M APTS in 15% glacial acetic acid) and 1.5 μL of sodium cyanoborohydride. After centrifugation at 4000 × *g* for 2 min, the mixture was incubated at 60 ℃ for 1 h 30 min in the dark. 80 μL of deionized water was then added and samples were vortexed until all precipitate was dissolved, then centrifuged at 4000 × *g* for 2 min. An aliquot of 50 μL was transferred to a FACE micro-vial for analysis with a P/ACE MDQ plus system (Ab Sciex, US). The resulting data are shown as the relative abundance of chains for each degree of polymerization (abbreviation DP, symbol *X*), as $N_{de}(X)$, the number distribution of chains with DP *X* after debranching.

2.5 Molecular size distributions using size-exclusion chromatography

Molecular size distributions of mouse-liver glycogen molecules were obtained using an aqueous size-exclusion chromatography (SEC) system [22]. Briefly, glycogen samples (1 mg/mL) were dissolved in a thermomixer at 80 ℃ for 3 h in 50 mmol/L ammonium nitrate/0.02% sodium azide. Samples were added to an Agilent 1260 Infinity SEC system (Agilent, Santa Clara, CA, USA) using a SUPREMA pre-column, joined to 1000 and 10,000 columns (Polymer Standards Services (PSS), Mainz, Germany) in series. The columns were kept at 80 ℃ and the flow rate was set to 0.3 mL/min. A refractive index detector (Optilab UT-rEX, Wyatt, Santa Barbara, CA, USA) was used to determine the relative weight of molecules as a function of elution volume [23]. An SEC universal calibration curve was constructed using pullulan samples (PSS), with a molar mass range of 342-2.35 × 10^6 Da, thereby allowing the elution volume, which is an instrumental quantity, to be converted to a molecular quantity, the hydrodynamic radius R_h of the starch molecules. The data from the DRI detector are presented here as the SEC weight distribution as a function of R_h, w (log R_h).

2.6 Transmission electron microscopy

Glycogen morphology was observed by transmission electron microscopy (TEM), using a previously-reported method [24]. Glycogen was resuspended in 50 mmol/L Tris-HCl buffer (pH 7.0) at 1 mg/mL. Copper grids with carbon film were discharged for 30 s, using a Harrick plasma cleaner PDC-32G-2, before use. The glycogen solutions were diluted 10-fold, then a drop was placed on the grid for 3 min. Excess sample was drawn off using filter paper and the grid was stained with one drop of 2% uranyl acetate. The morphology of the starch was examined using an HT7800 transmission electron microscope (Thermo Fisher Scientific, Waltham, Mass., USA) operating at 80 kV.

2.7 Gene/protein-level detection

PolyA-selected mRNA from liver was fragmented, reverse-transcribed, and sequenced on Illumina NovaSeq (150-bp PE, 6 Gb/sample). Reads were quality-filtered (fastp), aligned to GRCm39 (HISAT2), and quantified (featureCounts). Real-time PCR analyses were conducted by a published method [25]. For western-blot analysis, tissue samples were extracted using RIPA lysate containing protease inhibitor cocktail, and an immunoblot assay of the proteins in the liver was performed as previously described [17]. Specifically, frozen liver samples were homogenized in RIPA lysis buffer containing 1% protease inhibitor cocktail (Beijing Solarbio Science & Technology Co., Ltd.). The supernatant was collected after centrifugation (12000 × g at 4 ℃ for 15 min), and the total protein concentration was quantified using the BCA Protein Colorimetric Assay Kit (Elabscience Biotechnology Co., Ltd.), followed by mixing with loading buffer. Equal amounts of proteins (40 μg) were separated by electrophoresis on 10 % SDS polyacrylamide gels and transferred to nitrocellulose membranes (Millipore, Bedford, MA). Membranes were blocked for 1 h at room temperature with 5% skimmed milk in TBST. The membranes were then incubated with primary antibodies against PYGL-phospho S15 (ab227043, Abcam), AGL (ab133720, Abcam), PPP1R3B (27285-1-AP, Proteintech), GBE1 (A6599, Abclonal) and GYS1 (10566-1-AP, Proteintech) at a dilution ratio of 1:1000.

The membranes were washed three times and incubated for 1 h at room temperature in TBST with anti-rabbit or anti-mouse HRP-conjugated secondary antibodies at a dilution ratio of 1:10000. The membranes were then treated with enhanced chemiluminescence (ECL, Thermo Scientific). Densitometry analysis was performed using the publicly-available image analysis software package Image J (National Institutes of Health, Bethesda, MD, USA).

2.8 Statistics

Histological scoring and glycogen structural analyses were performed by investigators blinded to treatment groups. Statistical analysis plans were established a priori to avoid selective reporting. When comparing between two groups (e.g. mice with or without MASH), we used an unpaired t-test. When comparing three or more groups (e.g. MASH mice treated with three hepatoprotective polyphenols compounds), we used a one-way ANOVA with Tukey's multiple comparison test. Statistical analysis was performed in GraphPad Prism 10. Quantification of all staining was performed using ImageJ, by measuring the positive staining area or integrated density in multiple randomly selected fields (data were expressed as means ± SE or means ± SD). Significant differences in the mean values were determined at $P < 0.05$.(*P <0.05; **P <0.01, ***P <0.001, ****P <0.0001). All raw data and analysis scripts are available upon request to facilitate independent verification.

3. Results

3.1 Glycogen architecture dysregulation in MASLD

3.1.1 Serum/liver indicators and tissue histology in MASLD

To model MASLD, we administered a high-calorie HFD to mice for an extended period. As anticipated, these animals exhibited modest elevations in serum ALT and AST, though not reaching statistical significance, consistent with mild, early-stage hepatocellular injury within the MASLD spectrum, whereas fasting blood glucose was markedly increased and body weight was significantly higher (Figure 1A). Histological analysis revealed pronounced hepatic steatosis on H&E staining, whereas Masson trichrome staining showed no evidence of fibrosis (Figure 1B). Consistent with impaired hepatic glucose metabolism, both biochemical assays and PAS staining demonstrated a significant reduction in hepatic glycogen content in MASLD mice, relative to normal controls.

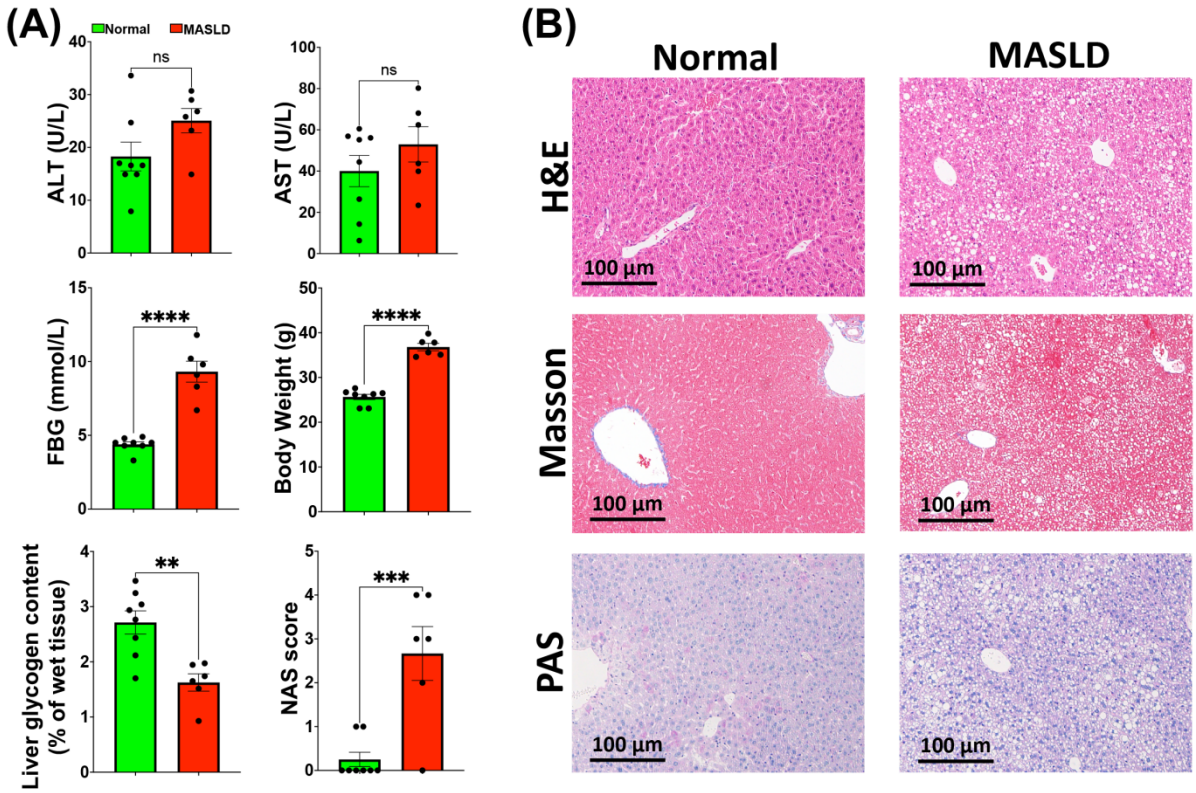


Figure 1. Serum biochemistry and liver histology in MASLD mice**.** (A) Serum ALT/AST levels, FBG, body weight, hepatic glycogen content and NAS score; (B) H&E, Masson and PAS staining of liver tissue. Data are presented as means ± SEM (n=6-8); unpaired t-test was employed to compare two groups, $^{**}P$ <0.01, $^{***}P$ <0.001, $^{****}P$ <0.0001.

3.1.2 Liver glycogen CLDs, molecular size distributions and density distributions in MASLD

Liver glycogen structure results for MASLD mice are shown in Figure 2. Panels A and B show the CLDs of liver glycogen in MASLD, and of healthy (control) mice. The trend from the average curve suggests a moderate increase in the relative amount of long-chain glycogen in MASLD mice compared to the controls. Panel C shows the average chain lengths (ACLs), $(\Sigma_X X N_{de}(X))/ (\Sigma_X N_{de}(X))$, of the two groups. Although the MASLD group showed a slightly higher ACL (6.5 ± 1.1) than controls (6.2 ± 0.7) without reaching statistical significance, the distribution curve consistently revealed an elevated proportion of long chains (Figure 2A), a trend that progressed to a significant difference in the MASH stage (Figure 5J).

Panels C and D show the molecular size distribution of liver glycogen before and after DMSO treatment in MASLD and the control groups. There was no obvious fragility in glycogen in either group upon DMSO treatment, as most α particles did not degrade significantly into smaller β particles. β particles are defined here as that portion of the distribution with R_h < 30 nm. Based on the area under the curve (AUC) above the minimum at ~10 nm, the β-particle content was calculated as AUC (R_h < 30 nm)/AUC (total R_h) [26].

From the β-particle content, mean $\bar{R}_h$ and $R_{h,max}$ (Panels E and F), it was confirmed that both groups were largely resistant to DMSO treatment. For completeness, we also report that the healthy control group had significantly lower β-particle content ((32.6 ± 3.8) %) than the DMSO-treated MASLD group ((40.7 ± 5.8) %) (one-way ANOVA with Tukey's test: $^{*}P$ <0.05). In contrast, the mean $\bar{R}_h$ ((30.9 ± 0.8) nm) and

$R_{h,max}$ ((36.5 ± 0.5) nm) values of the control group were significantly higher than those of the DMSO-treated MASLD group (mean $\bar{R}_h$: (28.9 ± 1.4) nm; $R_{h,max}$: (35.3 ± 1.0) nm) (one-way ANOVA with Tukey's test: *P <0.05).

Direct comparison between untreated MASLD and control groups via an unpaired t-test revealed that the MASLD group had significantly higher β-particle content ((39.2 ± 5.4) %, P = 0.03), but lower mean $\bar{R}_h$ ((30.5 ± 1.3) nm, P = 0.045) and $R_{h,max}$ ((35.7 ± 0.8) nm, P = 0.03). Thus, while glycogen α particles in MASLD mice did not exhibit obvious fragility, the MASLD group had consistently higher β-particle contents than those of the control group.

Panels G and H illustrate the molecular density of each group before and after DMSO treatment. Both healthy and MASLD groups showed a tendency toward reduced density after DMSO treatment. Panel I presents the maximum density and mean density across groups. Consistent with the β-particle content and R_h results, the maximum density of glycogen in the MASLD group with DMSO treatment ((0.26 ± 0.09) g/cm^3) was significantly lower than that of the control group ((0.30 ± 0.05) g/cm^3) (one-way ANOVA with Tukey's test: *P <0.05).

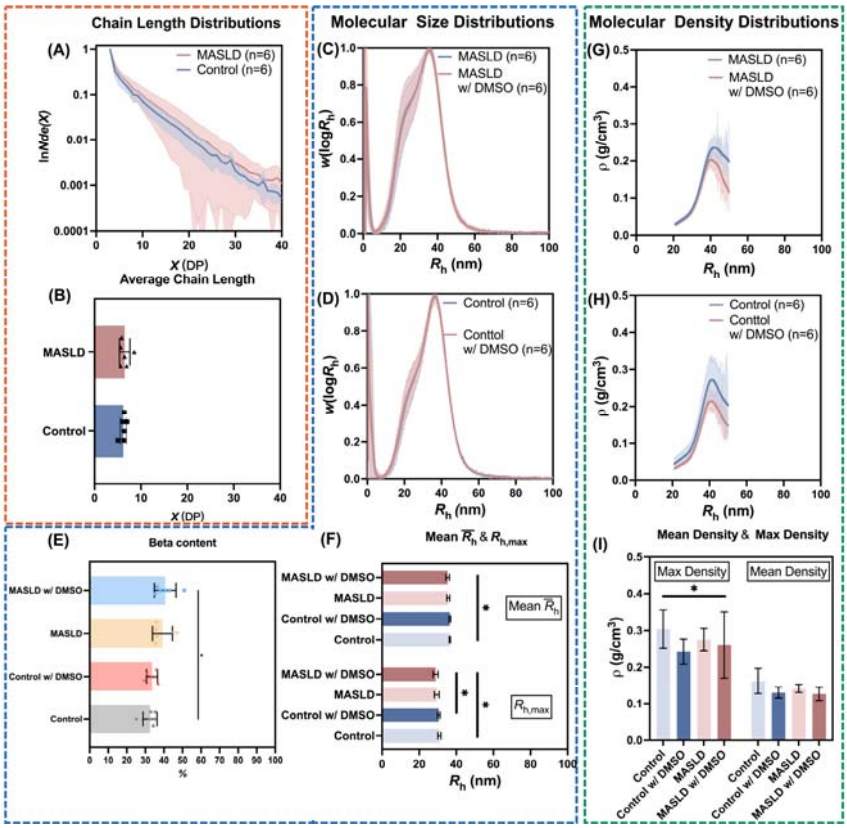


Figure 2. Liver glycogen CLDs, molecular size distributions, and molecular density distributions of MASLD mice and healthy controls. (A) number CLDs, $N_{de}(X)$, of liver glycogen from mice. Curves show the mean of 6 biological replicates with SD error bars. Red: MASLD samples; blue: healthy controls without MASLD. (B) mean chain length of each group. (C-D) molecular size distributions of liver glycogen, normalized to have the same maximum $w(\log R_h)$. Curves represent the mean at a given R_h, with the SD provided on either side of the main line (n = 6). Red: MASLD or control samples with DMSO treatment; Blue: MASLD or control samples without DMSO treatment. (E) the glycogen β-particle content of each group. (F) $\bar{R}_h$ and $R_{h,max}$ for each group. (G-H) molecular density distributions of liver glycogen. Curves represent the mean at a given R_h, with the SD provided on either side of the main line (n = 6). Red: MASLD or control samples with DMSO treatment; Blue: MASLD or control samples without DMSO treatment. (I) mean and maximum densities of each group. Statistical significance of Panel B: unpaired t-test; Panels E, F, I: one-way ANOVA with Tukey's multiple comparison test. *P <0.05, **P <0.01, ***P <0.001, ****P <0.0001.

3.1.3 Glycogen metabolism signaling in MASLD

Transcriptome data show that the hepatic glycogen-metabolism gene profile is reprogrammed in MASLD mice (Supplemental Figure 1-5), while GO and KEGG enrichment show the involvement of the PI3K-AKT and PPAR pathways in this metabolic shift. Based on the broad disturbances observed in metabolic pathways from the transcriptomic analysis and given the central roles of AGL, GBE1, GYS1, PYGL and PPP1R3B in glycogen-structure regulation, we next sought to determine whether the expression of these key factors was altered at the protein level in MASLD livers. Compared with normal controls, MASLD mice exhibited elevated hepatic expressions of AGL, GBE1, and PYGL, whereas those of GYS1 and PPP1R3B remained unchanged (Figure 3). Collectively, the concurrent up-regulation of both glycogenic and glycogenolytic enzymes indicates a profoundly dysregulated glycogen homeostasis in MASLD. While GBE1 is not a rate-limiting enzyme, PYGL is a key rate-limiting enzyme in glycogen degradation, and its marked up-regulation provides a mechanistic explanation for the reduced glycogen content observed in MASLD livers.

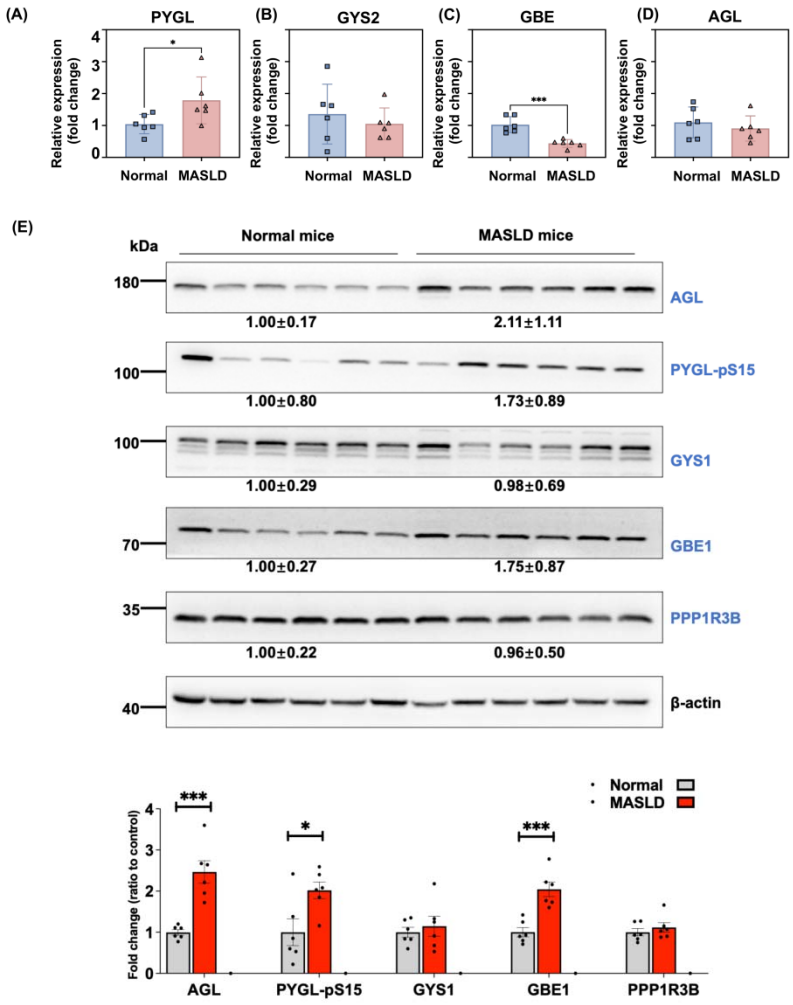


Figure 3. Hepatic glycogen homeostasis-related protein expression in MASLD mice. (A-D) hepatic mRNA levels of PYGL, GYS2, GBE and AGL between normal control group and MASLD group; all mRNA levels are normalized to *β*-actin and expressed relative to the normal control group; (E) representative western blot bands for AGL, GBE1, GYS1, PYGL and PPP1R3B in liver lysates from control and MASLD mice, as well as densitometric quantification normalized to internal reference. Data are presented as means ± SEM (n=6); unpaired t-test was employed to compare two groups, **P* <0.05, ***P* <0.01.

Table 1. Biochemical analysis of MASH mice.

	CG	MASH	QR	NAG	LTL
Serum ALT (U/L)	6.2±2.8^{c}	72±20^{a}	56.5±24.9^{a,b}	78.4±29.4^{a}	34.5±3.3^{b,c}
Serum AST (U/L)	43.7±16.8^{b}	102±14^{a}	100.2±32.9^{a}	66.0±8.3^{b}	73.1±9.2^{a,b}
Hepatic TG (mmol/mg prot)	0.9±0.2^{b}	2.4±0.9^{a}	1.6±0.7^{a,b}	1.4±0.6^{a,b}	1.8±0.3^{a,b}
Hepatic TC (mmol/mg prot)	1.0±0.2^{b}	2.3±1.0^{a}	1.7±0.8^{a,b}	1.5±0.4^{a,b}	1.8±0.6^{a,b}
GSH (mmol/mg prot)	14.8±4.7^{a}	13.2±5.4^{a}	17.6±8.5^{a}	20.1±7.0^{a}	21.6±5.0^{a}
MDA (mmol/mg prot)	3.3±1.2^{b}	18.2±9.6^{a}	10.7±2.1^{a,b}	6.6±3.5^{b}	6.1±1.3^{b}
FBG (mmol/L)	3.8±1.2^{a}	3.4±1.0^{a}	2.9±0.3^{a}	4.0±2.1^{a}	2.5±1.0^{a}
Body weight (g)	24.0±1.3^{a}	14.8±0.8^{b}	14.8±0.9^{b}	15.1±0.7^{b}	15.4±0.8^{b}
Wet liver weight (g)	1.0±0.2^{a}	0.5±0.09^{c}	0.6±0.1^{b,c}	0.6±0.1^{b,c}	0.7±0.1^{b}
Liver glycogen content (% of wet tissue)	7.5±1.3^{a,b}	9.6±1.6^{a}	7.7±1.6^{a,b}	8.0±3.1^{a,b}	6.3±1.3^{b}
Liver index (%)	4.1±0.7^{a,b}	3.5±0.6^{b}	4.1±0.8^{a,b}	3.9±0.7^{a,b}	4.6±0.6^{a}

Note: values are the mean ± SD (n = 5-10). The liver index is the ratio of liver weight to body weight. Differences in values with different letters in the same row are statistically significant, as measured with a one-way ANOVA with Tukey's multiple comparison test (P <0.05).

3.2 Glycogen architecture dysregulation in MASH

3.2.1 Serum/liver indicators and tissue histology

MASH is the progressive, inflammatory stage of the MASLD spectrum, and is markedly more severe than the initial stage of MASLD (simple steatosis). In our animal model, MASH mice exhibited significantly higher serum ALT and AST activities than their normal control counterparts, consistent with advanced hepatocellular injury (Table 1, Supplementary Table 2). Hepatic lipid accumulation was evident in both biochemical assays (elevated hepatic TG and TC) and histological analyses (H&E and ORO staining, Figure 4). Furthermore, hepatic MDA levels were substantially elevated compared with normal controls, reflecting heightened oxidative stress. Notably, unlike MASLD mice, MASH mice that had been fed the MCD diet did not display increased FBG; instead, they exhibited augmented hepatic glycogen content (Table 1, Figure 4), indicating that glycogen homeostasis might be reprogrammed as the disease transitions to the inflammatory phase.

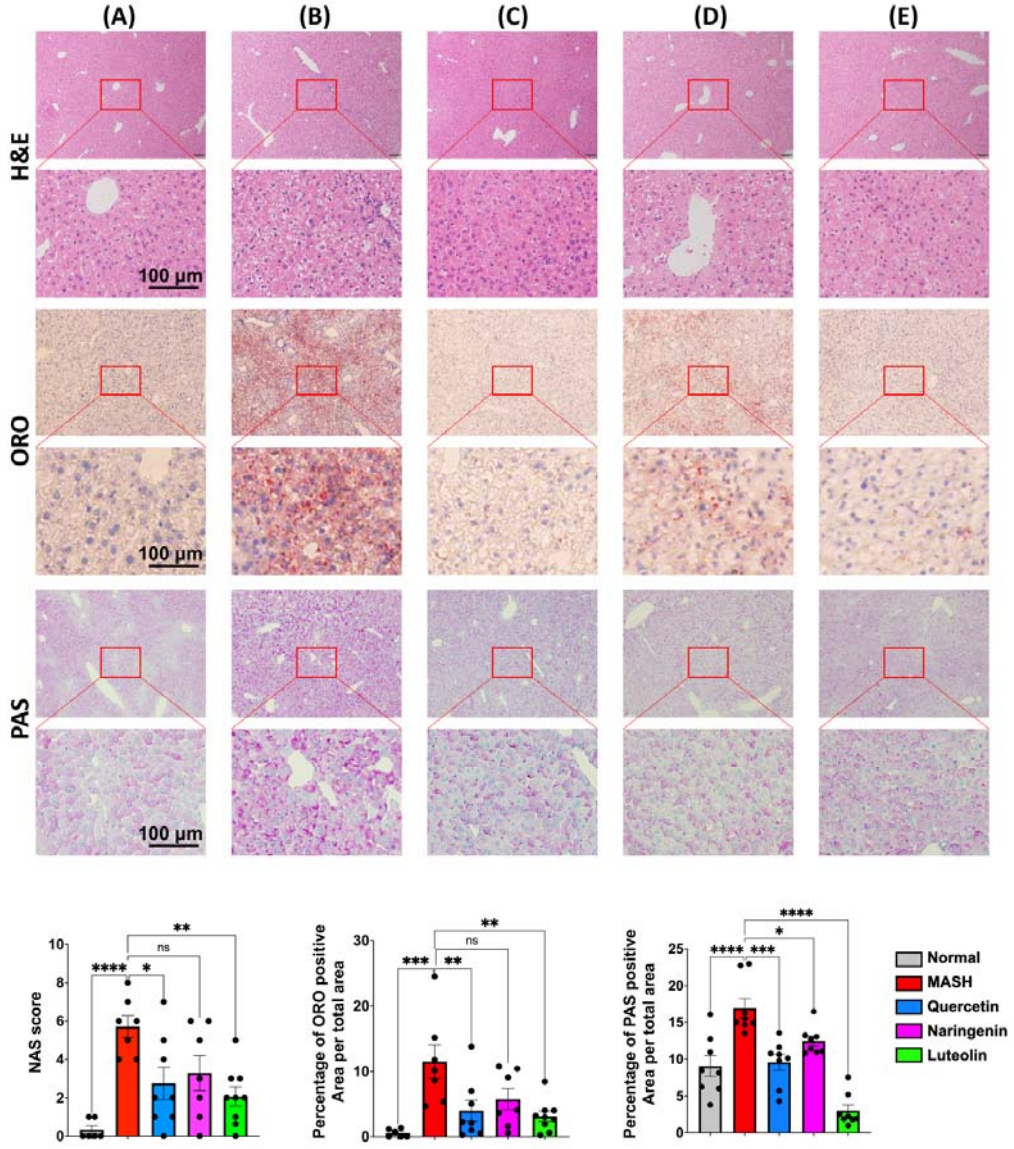


Figure 4. Representative H&E, ORO, and PAS-stained slices images of livers. (A) Normal control group; (B) MASH group; (C) Experimental group 1 treated with quercetin; (D) Experimental group 2 treated with naringenin; (E) Experimental group 3 treated with luteolin. Data are presented as means ± SEM (n=8); a one-way ANOVA with Tukey's multiple comparison test was employed to compare different groups, **P* <0.05, ***P* <0.01, ****P* <0.001, *****P* <0.0001. Red squares indicate the enlarged areas.

3.2.2 Liver glycogen CLDs, molecular size distributions and TEM in MASH with and without treatment by hepatoprotective compounds

The liver glycogen CLDs and molecular size profiles of MASH mice with and without treatment with three hepatoprotective compounds are shown in Figure 5. Panels A-D show the CLDs of liver glycogen in healthy control and in MASH mice with and without treatment. Samples from the MASH groups exhibited a higher proportion of longer chains compared to the controls. Panel J displays the ACLs across groups. The ACL of the control group was significantly smaller than those of all MASH groups, regardless of treatment (Tukey's multiple comparison test: CG vs. MASH, P <0.0001; CG vs. QR, P = 0.0005; CG vs. NAG, P = 0.0001; CG vs. LTL, P = 0.0032), indicating that MASH mice possess significantly more long-chain glycogen than those of healthy controls. Notably, the ACLs of MASH mice treated with quercetin or luteolin

were significantly reduced compared to the untreated MASH group (Tukey's test: QR vs. MASH, P = 0.045; LTL vs. MASH, P = 0.008).

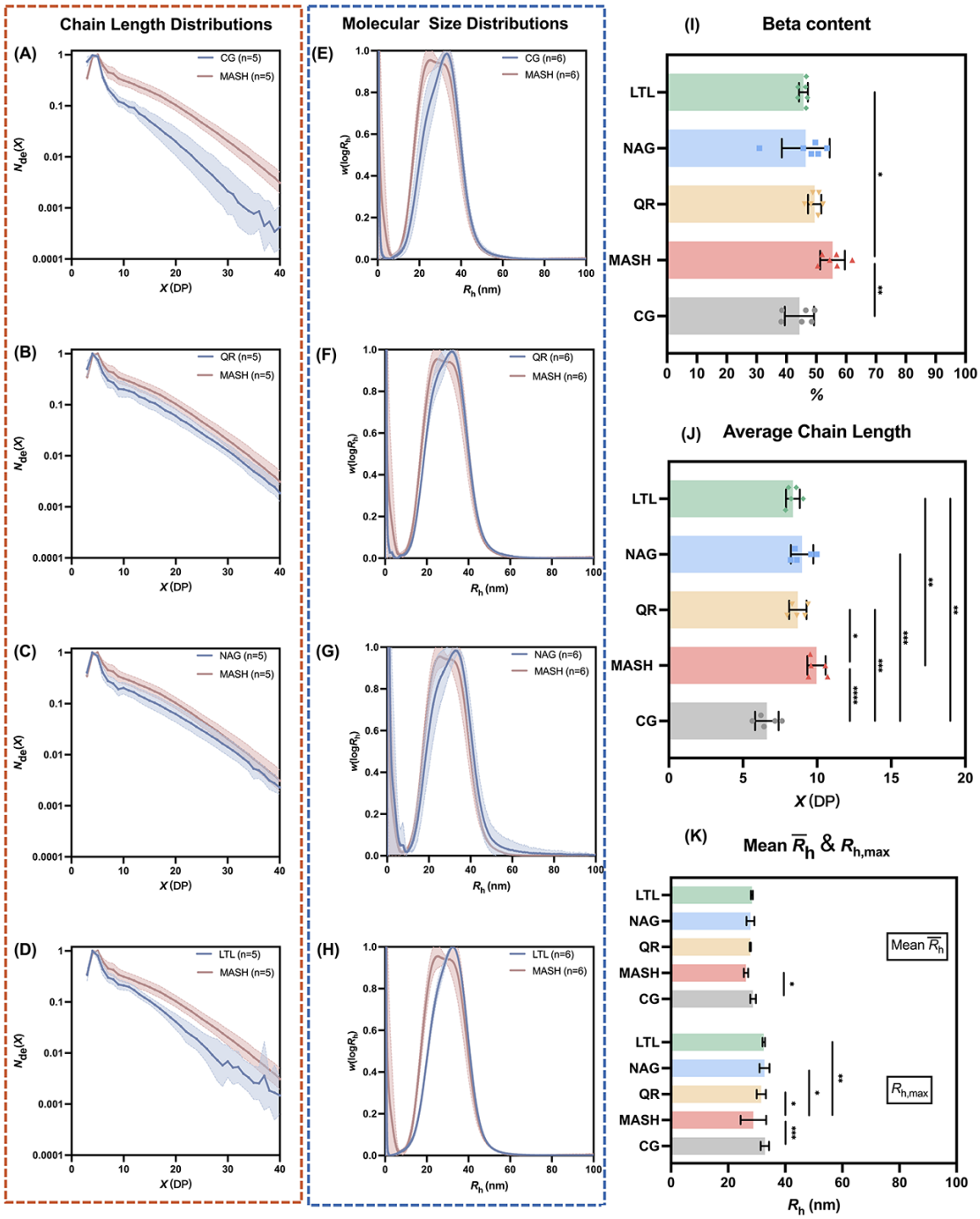


Figure 5. Liver glycogen CLDs, molecular size distributions of healthy controls, MASH mice, and MASH mice treated with quercetin (QR), naringenin (NAG), and luteolin (LTL). Panels A-D: $N_{de}(X)$ of liver glycogen from mice. Curves show the mean of 5 biological replicates with SD error bars. Red: MASH samples (Panel A-D); Blue: MASH samples treated with QR (Panel B), naringenin (NAG) (Panel C), luteolin (LTL) (Panel D), and healthy controls without MASH (Panel A). Panels E-H: molecular size distributions, $w(\log R_h)$, of liver glycogen, normalized to have the same maximum. Curves represent the mean at a given R_h, with the SD provided on either side of the main line (n = 6). Red: MASH samples; Blue: MASH samples treated with quercetin (QR) (Panel F), naringenin (NAG) (Panel G), luteolin (LTL) (Panel H), and without MASH (Panel E). Panel I represents the glycogen β-particle content of each group. Panel J: mean chain length of each group. Panel K: R_h and $R_{h,max}$ for each group. Statistical significance was determined by one-way ANOVA with Tukey's multiple comparison test: *P <0.05, **P <0.01, ***P <0.001, ****P <0.0001.

Panels E-H show the molecular size distributions of liver glycogen control and MASH groups with and without the treatment with three hepatoprotective compounds. Compared to the untreated MASH group, both the healthy control, and the MASH groups treated with hepatoprotective compounds, showed a shift in the average curve toward larger particles, i.e. a higher proportion of α particles. Panel K and I show mean $\bar{R}_h$, $R_{h,max}$ and β-particle content for each group. The untreated MASH group had significantly smaller $\bar{R}_h$ and $R_{h,max}$ values than those of the control group (Tukey's test: $\bar{R}_h$, CG vs. MASH, P = 0.0003; $R_{h,max}$, CG vs. MASH, P = 0.05). The $\bar{R}_h$ values of all treated MASH groups were significantly larger than those of the untreated MASH group and were not significantly different from the control group. The $R_{h,max}$ values of all treated MASH groups showed no significant differences compared either to the control group or the untreated MASH group. The untreated MASH group had the highest β-particle content among all groups, which was significantly greater than that of the naringenin- and luteolin-treated MASH groups and the non-disease group (Tukey's test: CG vs. MASH, P = 0.0038; NAG vs. MASH, P = 0.023; LTL vs. MASH, P = 0.012). However, no significant difference was observed in β-particle content between the quercetin-treated and untreated MASH groups (Tukey's test: QR vs. MASH, P = 0.22).

Representative TEM micrographs of hepatic glycogen particles from control and MASH mice, with or without treatment, are shown in Figure 6. Both β particles (<30 nm) and α particles (30-300 nm) were observed in all groups, consistent with the SEC molecular size distributions.

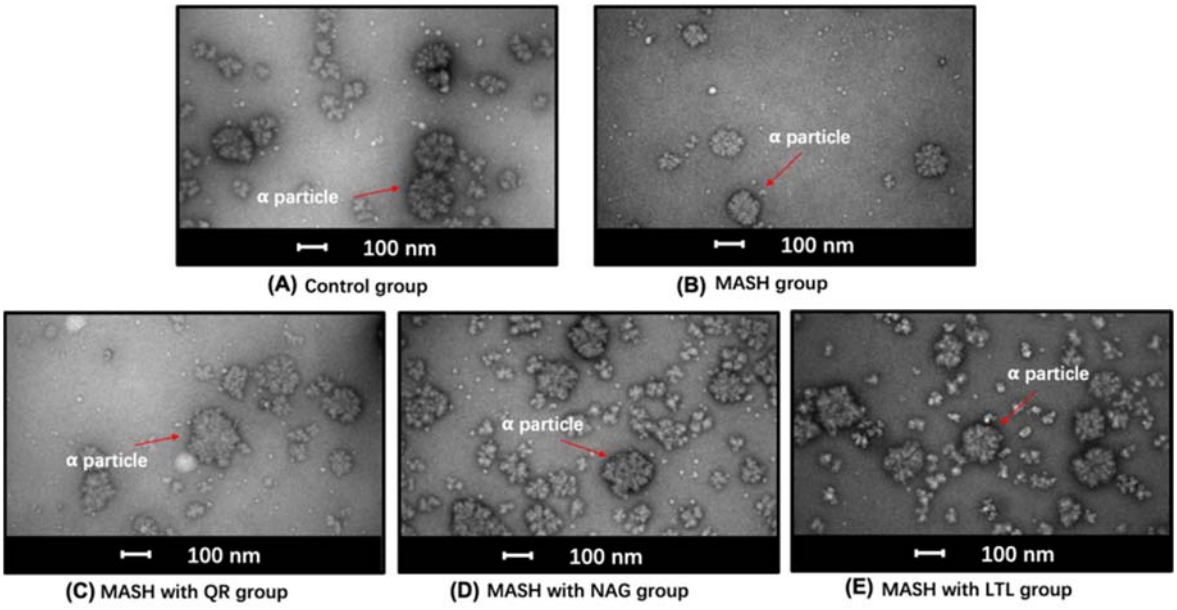


Figure 6. Ultrastructural characterization of hepatic glycogen architecture via TEM. Representative TEM images revealing the sub-cellular morphology of liver glycogen in different experimental models. (A) Control group: Characterized by well-organized, high-density, cauliflower-like α particles. (B) MASH group: Demonstrates severe architectural impairment, with large α particles fragmented into scattered, smaller β subunits or degraded clusters. (C) MASH + Quercetin (QUE), (D) MASH + Naringenin (NAR), and (E) MASH + Luteolin (LUT): Intervention with these bioactive compounds significantly preserves the integrity of glycogen architecture, promoting the restoration of robust α particle clusters and reducing particle fragmentation compared to the MASH group. Scale bars = 100 nm.

3.2.3 Glycogen metabolism signaling in MASH

As noted above, during the transition from mild MASLD to severe MASH, hepatic glycogen levels followed divergent trajectories, likely reflecting a shift from compensatory protection to injury-driven

depletion. However, it is interesting to find that glycogen architecture exhibited a uniform signature: progressively longer chains and a higher proportion of β particles that became more pronounced as liver injury intensified. We therefore examined how the proteins governing glycogen homeostasis were reprogrammed across this spectrum. Our results demonstrate that the expression levels of AGL, GBE1, PYGL, and GYS1 were consistently lower in MASH mice relative to controls (Figure 7). Notably, these key glycogen-related proteins exhibited a opposite trend in the MASH model compared to the MASLD phase. While MASLD is characterized by a significant elevation of these enzymes, the progression to the more severe MASH phenotype results in a profound downregulation. This reversal in protein expression trajectories underscores a critical metabolic shift in glycogen homeostasis as the disease advances from simple steatosis to inflammatory steatohepatitis.

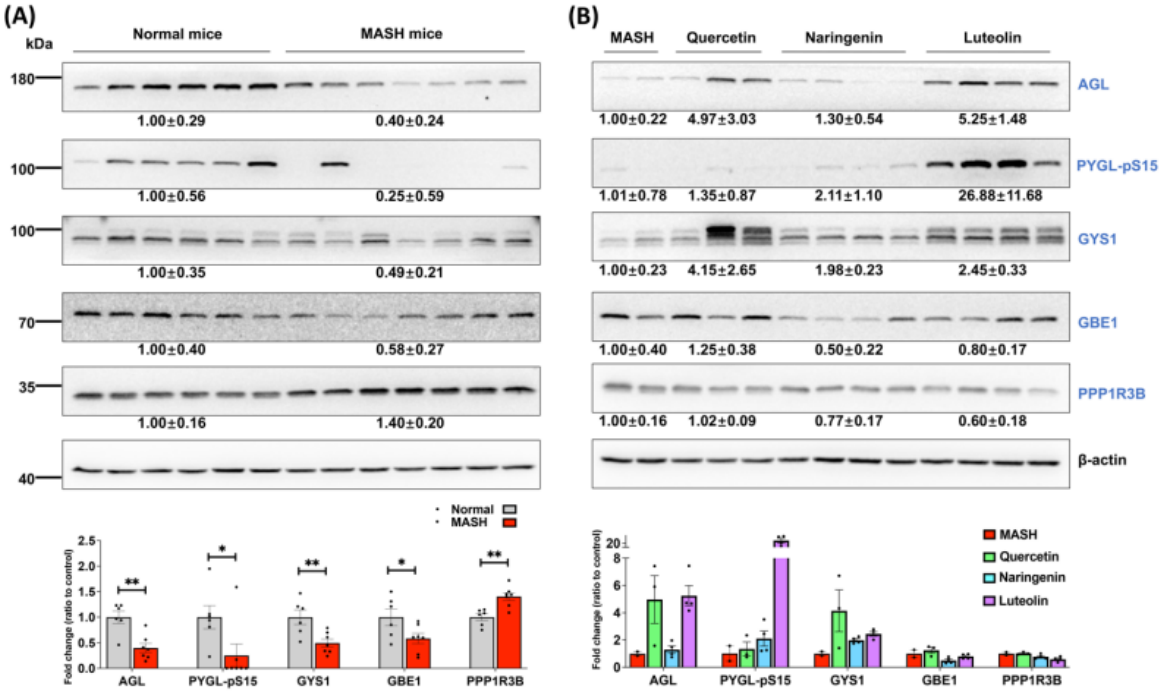


Figure 7. Hepatic glycogen homeostasis-related protein expression in MASH mice. Representative western blot bands for AGL, GBE1, GYS1, PYGL and PPP1R3B in liver lysates from (A) normal control and MASH mice, and (B) MASH mice and drug-treated MASH mice. Data in panel A are presented as means ± SEM (n=6); unpaired t-test was employed to compare two groups, *P <0.05, **P <0.01.

3.3 Therapeutic compounds change hepatic glycogen architecture and glycogen metabolic profile in MASH

3.3.1 Serum/liver indicators and tissue histology

The polyphenols quercetin, naringenin and luteolin share similar molecular structures and have all been shown to protect against MASH [17-19]. Consistent with previous reports, elevated serum ALT and AST levels in MASH mice can be partially reversed after intervention with any of these, demonstrating the anticipated hepatoprotective effects (Table 1). Likewise, treatment with quercetin, naringenin, or luteolin was seen to mitigate lipid deposition and oxidative stress in MASH mice (Table 1). As expected, hepatic steatosis (H&E staining), lipid accumulation (ORO staining) and hepatic glycogen deposition (PAS staining) in MASH mice were all significantly mitigated by intervention of the polyphenolic compounds (Figure 4).

Although these therapeutic polyphenols left FBG unchanged, they restored to normal the modestly elevated hepatic glycogen content observed in MASH mice, with treatment by luteolin achieving statistical significance (Tukey's multiple comparison test: MASH vs. LTL, $P = 0.02$).

3.3.2 CLDs and molecular size distributions

Treatment with quercetin, naringenin, or luteolin was associated with a significant amelioration of glycogen structural abnormalities in MASH mice. With respect to glycogen size distributions, all three polyphenolic compounds shifted hepatic glycogen toward the size distributions characteristic of larger α particles, a trend consistent with healthy controls and opposite to that observed in MASH. Similarly, in terms of CLD, all three treatments shortened longer glycogen chains and elongated shorter ones, although to varying degrees. Quercetin and luteolin elicited pronounced reductions in long-chain glycogen, whereas naringenin, though effective, resulted in a comparatively higher retention of longer chains. These structural improvements may suggest all three polyphenolic compounds produced a restoration of dynamic homeostasis and functional integrity in glycogen metabolism. An increased prevalence of α particles with shorter chains, which are more stable and less prone to degradation into β particles than their long-chain counterparts [9], may help preserve hepatic energy stores, reduce ER stress, and limit inflammatory responses, thereby ameliorating MASH-related liver damage.

3.3.3 Polyphenol-mediated regulation of glycogen metabolism in MASH

The three dietary polyphenols exhibited distinct regulatory profiles on glycogen-metabolizing proteins compared to the MASH model group. Specifically, quercetin treatment significantly upregulated the protein abundance of AGL and GYS1. Luteolin primarily enhanced the expression of PYGL and AGL, while naringenin treatment resulted in a modest increase in the levels of PYGL and GYS1 (Figure 7). This divergence indicates that while these polyphenols collectively restore glycogen architecture, they may exert their therapeutic effects through distinct enzymatic nodes within the glycogen homeostatic network.

Molecular docking simulations demonstrated strong binding affinities between these polyphenols and various AMPK isoforms, indicating their potential role as common upstream regulators (Figure 8A). This hypothesis was preliminary validated *in vitro*, where the inhibition of AMPK by Compound C significantly interfered with the polyphenols' regulatory effects on AGL, PYGL, and GYS1, suggesting that AMPK is a critical mediator in the remodeling of glycogen metabolic enzymes (Figure 8B). *In vivo* experiments further showed that hepatic p-AMPK expression was markedly suppressed in MASH mice, whereas polyphenol intervention restored its phosphorylation levels to varying degrees, alongside the downregulation of the ER stress marker GRP78 (Figure 8C). While AMPK serves as a key regulator of glycogen-related proteins, the specific molecular mechanisms and downstream signaling pathways triggered by these polyphenols require further exploration.

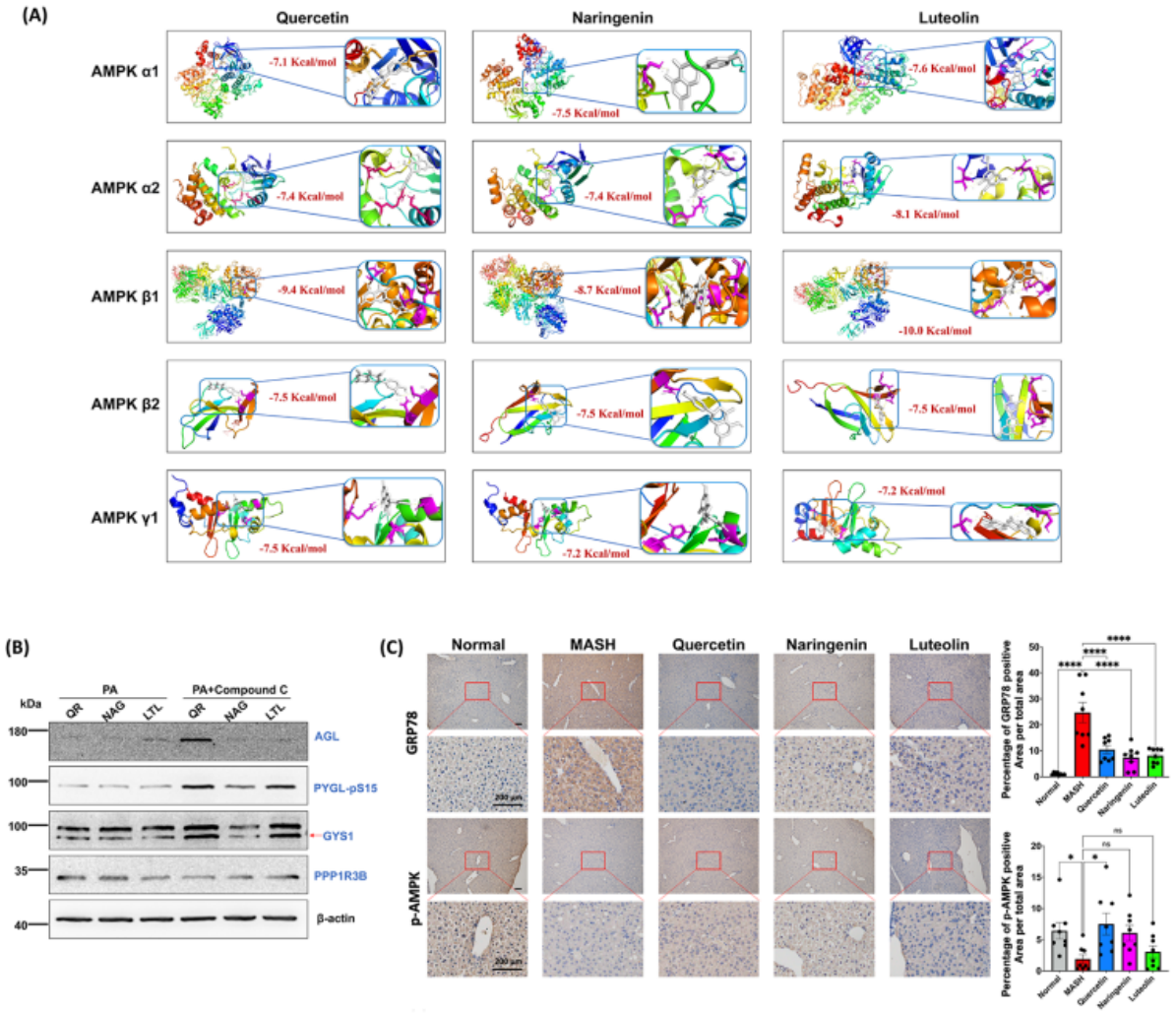


Figure 8. The role of AMPK in the intervention of quercetin, naringenin or luteolin. (A) Molecular docking between different subtypes of AMPK and quercetin/naringenin/luteolin; a binding energy ≤ -8.0 kcal/mol indicates strong binding; -8.0 kcal/mol < binding energy ≤ -6.0 kcal/mol indicates moderate binding; and binding energy > -6.0 kcal/mol indicates weak binding. (B) Western blot bands from in vitro experiments using the NCTC 1469 cell line. Cells were treated with 200 μmol/L palmitic acid to induce the MASH phenotype, and co-cultured with 20 μmol/L quercetin, naringenin, or luteolin, either with or without compound C. For compound C pretreatment, cells were incubated with 10 μmol/L compound C for 2 hours prior to the subsequent drug or palmitic acid treatment. (C) Representative immunohistochemical staining of hepatic GRP78 and p-AMPK protein from MASH mice with and without treatment by three hepatoprotective polyphenols, and non-diseased controls; scale bar indicates 200 μm; data are presented as means ± SEM (n=8); a one-way ANOVA with Tukey's multiple comparison test was employed to compare different groups, **P* <0.05, *****P* <0.0001.

4. Discussion

MASLD encompasses a broad continuum, extending from simple steatotic MASLD to inflammatory MASH, and can ultimately advance to fibrosis, cirrhosis, and even hepatocellular carcinoma. At present, no single murine model faithfully echoes the full spectrum of human MASLD. In this study, we therefore employed the widely used HFD to induce the early-phase simple steatosis and the MCD diet to trigger inflammatory-phase MASH. HFD alone produces hepatic steatosis without overt inflammation, whereas the MCD diet is a potent, albeit severe, regimen that rapidly elicits hepatic inflammation. Notably, MCD feeding causes marked weight loss and hypoglycaemia, features that diverge from the typical metabolic profile observed in human MASH [27]. Although no perfect animal model completely recapitulates all

aspects of human MASH pathophysiology, the MCD diet-induced model represents a well-established and widely-accepted classical approach for investigating hepatic inflammation and metabolic dysfunction [28, 29]. While MCD-fed mice lack the obesity phenotype and metabolic syndrome features characteristic of human MASH, the fundamental biological processes governing glycogen metabolism, hepatocyte architecture, and inflammatory signaling operate through conserved molecular mechanisms that are model-independent [30, 31]. Recent comprehensive studies have demonstrated that MCD diet-induced MASH models effectively recapitulate hepatic pathological features and metabolic alterations observed in humans, including impaired glycogen metabolism and hepatic immune cell infiltration [29, 32]. Therefore, our findings regarding glycogen-architecture changes in the MCD-induced MASH model are biologically relevant and translationally significant, as the underlying mechanisms of hepatic metabolic dysfunction and inflammation are conserved across species and disease models. Moreover, the consistent finding of glycogen architectural disruption across these two mechanistically distinct models in the present study suggests that this phenomenon is a fundamental, convergent consequence of hepatic metabolic stress, rather than a model-specific artifact. This strengthens its potential biological relevance to human disease.

Our results reveal that hepatic glycogen structural remodeling initiates as early as the MASLD stage, prior to the onset of severe inflammation. In MASLD mice, hepatic glycogen is characterized by a significant shift toward a higher proportion of smaller β-particles, even as the ACL remains relatively stable. These findings suggest that early-stage MASLD is primarily marked by glycogen particle disaggregation and size reduction, reflecting a preliminary loss of structural integrity where the molecular branching pattern (represented by the ACL) has not yet been significantly altered. As the disease progresses to MASH, the structural dysregulation becomes more profound, manifested by a distinct architectural shift: a further accumulation of β-particles accompanied by a significant elongation of ACL. This specific combination increases the surface-to-volume ratio of the glycogen. This structural configuration predisposes the glycogen to accelerated and uncontrolled glycogenolysis, which likely drives excessive glucose output and exacerbates systemic metabolic dysfunction. Our data indicate that ACL elongation serves as a hallmark of the inflammatory stage, marking the transition from simple size redistribution to a fundamental aberration in the glycogen branching architecture.

While both MASLD and MASH exhibit a shared structural signature of elongated glycogen chains and increased β-particle content, they display opposing trends in glycogen-metabolic enzyme expression. We observed that the progression from MASLD to MASH is characterized by a persistent and even aggravated glycogen structural abnormality (elongated chains, increased β-particle ratio), while the protein expression patterns of its core regulatory enzymes (e.g., GYS1, GBE1) undergo reversal or lack consistent changes (Figure 3, Figure 7F). This decoupling phenomenon suggests that under pathological conditions, the determinants of glycogen architecture may shift from enzyme abundance to a reconfigured balance of enzyme activities, reshaped by overarching signals such as insulin resistance, inflammation, and ER stress. These signals may alter the functional output of key enzymes (e.g., GYS1, GBE1) through post-translational

modifications, leading to reduced net branching and chain elongation despite variable protein expression levels.

While the mRNA and protein expressions of PYGL and GYS were largely congruent in our model, GBE1 and AGL exhibited a striking paradoxical divergence. Such mRNA-protein uncoupling is a well-documented phenomenon under chronic metabolic stress, where steady-state protein abundance is increasingly dictated by translation efficiency and protein turnover rather than *de novo* transcription. In the pathological milieu of MASH, the accumulation of GBE1 and AGL proteins likely reflects a failure in protein degradation machinery, such as the autophagy-lysosomal or ubiquitin-proteasome pathways, which are typically compromised in steatohepatitis. Crucially, protein abundance is not a surrogate for enzymatic flux. Our structural data provided the definitive functional readout: the shift toward elongated α-chains and increased β-particle proportions serves as direct physical evidence that the branching activity is functionally insufficient. Consequently, the dysregulation of glycogen architecture in MASH represents a profound failure of functional enzymatic proteostasis rather than a simple transcriptional shift.

Polyphenols are plant-derived dietary compounds that have been postulated to protect against various metabolic and chronic diseases. Quercetin, naringenin and luteolin are representative polyphenolic compounds that have been demonstrated to be effective agents to treat MASH mice [19, 33, 34]. Our group has also demonstrated their efficacy in treating MASH (luteolin [19], quercetin [17], and naringenin [18]). Here, we leveraged these agents to determine whether changing hepatic glycogen architecture constitutes an integral mechanism underlying the therapeutic reversal of MASH. Our data showed that these therapeutic polyphenolic compounds affected the hepatic-glycogen structure of MASH-affected mice, partially returning the structural properties of the treated MASH mice to those of the non-diseased group. More specifically, the β-particle proportions of the MASH mice were decreased with all three treatments, returning to those of the non-diseased mice. The β-particle proportions from MASH mice with naringenin and luteolin treatments were significantly lower than those from the MASH mice without treatment. Although no MASH group with treatment had an ACL as small as that of the non-diseased group, the ACLs from the MASH group with quercetin and luteolin treatments were significantly smaller than those of the MASH group without treatment. Interestingly, the MASH group with luteolin treatment was the only one that had significantly different changes in both the glycogen sizes and chain lengths, compared to the MASH group without any treatment. This may indicate that luteolin has more beneficial effects on glycogen metabolism in MASH individuals than the other treatments. As mentioned above, the MASH groups with quercetin and luteolin treatments also had smaller ACLs than MASH group without treatment. Based on previous studies using diabetic mice [26], one hypothesis is that higher blood glucose is the factor resulting in increasing the glycogen average chain length. However, in this study, the MASH groups with naringenin treatments and those without treatments have blood sugar levels that are comparable to those of healthy controls. Therefore, it appears that variations in blood-sugar levels are not the only factor in influencing how glycogen structure is changed in MASH models. Although there are still a lot of unanswered questions on

how polyphenols affect glycogen, either directly or indirectly, this study may bring new directions for understanding the mechanisms of treatments of MASH disease, which may involve positive changes in glycogen structure and function.

Intriguingly, the three polyphenols showed divergent effects on individual enzyme expressions, such as the specific up-regulation of GYS1 by quercetin or the modulation of PYGL by luteolin, they all converge on a consistent structural restoration of hepatic glycogen. Given the inherent biological variations and the relatively limited sample size in our enzyme expression assays, these individual enzymatic shifts should be interpreted with caution. However, the uniformity of the architectural improvement suggests that these polyphenols might engage broader metabolic nodes that systemically reset glycogen homeostasis beyond the regulation of a single enzyme. One such potential candidate is AMPK, often regarded as a central metabolic sensor in hepatocytes [35]. Under physiological conditions, its phosphorylation simultaneously inactivates GYS2 and activates PYGL, restraining glycogen synthesis while promoting controlled glycogenolysis; it also concurrently phosphorylates ACC to shut down fatty-acid synthesis and boost β oxidation (this is the central step in fatty acid catabolism), in which fatty acids are broken down into acetyl-CoA to generate energy or enter the tricarboxylic acid (TCA) cycle. Previous literatures have demonstrated that quercetin, naringenin and luteolin re-activate AMPK through distinct upstream routes [17, 36-38]. Our molecular docking simulations hinted at a potential interaction, showing that quercetin, naringenin, and luteolin possess strong binding affinities for various AMPK isoforms (Figure 8A). This was further supported by our *in vitro* findings, where the chemical inhibition of AMPK using Compound C partially interfered with the polyphenols' ability to modulate AGL, PYGL, and GYS1 (Figure 8B). Furthermore, immunohistochemical analysis confirmed that the suppression of p-AMPK in MASH livers was restored to varying degrees following polyphenol intervention, alongside a reduction in the ER stress marker GRP78.

While these observations provide a putative link between AMPK and the preservation of glycogen macromolecular scaffolding, they do not constitute definitive proof of a direct causal relationship. The paradoxical finding that different polyphenols exert distinct molecular signatures on protein expression yet yield identical structural outcomes suggests a more complex systemic reprogramming of metabolic flux. It is possible that the restoration of glycogen architecture is a collective result of improved cellular homeostasis such as the relief of ER stress, rather than a response to a single signaling target. Therefore, while our data point toward AMPK as a potential orchestrator in this process, the precise molecular mechanism through which these diverse flavonoids converge on glycogen structural repair remains to be fully elucidated. These preliminary mechanistic insights serve as a foundation for future studies, which will require more advanced molecular biology tools such as cell-specific gene knockout models to verify the direct targets and downstream signaling hierarchies involved in hepatic glycogen homeostasis.

Overall, the glycogen structural signature in MASLD spectrum appears to emerge early in the disease process, potentially preceding overt liver damage indicated by elevated ALT and AST levels. The ability to differentiate MASLD from MASH based on glycogen architecture could significantly impact clinical

management, enabling targeted therapeutic interventions for MASH patients while avoiding unnecessary treatments for those with simple steatosis. However, the direct assessment of liver glycogen structure is invasive. Therefore, translating this finding into clinical practice necessitates the development of non-invasive detection methods. We propose the following avenues: (1) Exosome-Glycoprotein Panels: hepatocyte-derived exosomes may encapsulate glycogen granules and their associated regulatory enzymes. Detecting specific glycogen structural features or related glycoproteins within these exosomes could offer a minimally invasive biomarker. While exosome-based diagnostics are gaining traction in liver-disease research [39], the sensitivity and specificity of such panels for MASH, particularly concerning glycogen structure, remain to be established. Significant research is needed to standardize exosome isolation, identify robust exosomal markers, and validate their diagnostic accuracy in human cohorts. (2) Non-Invasive Imaging Techniques: Proton Magnetic Resonance Spectroscopy (^{1}H-MRS): ^{1}H-MRS is a valuable tool for quantifying hepatic glycogen content non-invasively *in vivo*. While standard ^{1}H-MRS primarily assesses overall glycogen amount, advanced MRI techniques may offer enhanced sensitivity to glycogen structure and spatial distribution, potentially enabling the detection of α- and β-particle ratios or chain-length abnormalities in vivo. (3) Dual-Mode Ultrasound-Photoacoustic Imaging: This modality offers high resolution and depth penetration, enabling the detection of liver metabolites. Research is ongoing to leverage photoacoustic imaging for monitoring metabolic changes in the liver, including the potential to characterize glycogen [40]. Further validation is required to confirm its ability to specifically detect glycogen structural alterations in MASH.

5. Limitations

It is important to note that this study is a discovery-phase investigation. While we identify a strong correlation between polyphenol treatment, AMPK modulation, and glycogen structural normalization, direct causal evidence remains to be established. Establishing glycogen architecture as a direct therapeutic target requires causal validation through genetic or pharmacological manipulation of specific enzymes, which is beyond the scope of this initial discovery study. Therefore, we have been careful to present this idea as a novel and testable hypothesis generated by our data, rather than as a proven conclusion.

Moreover, it must be acknowledged that the present study was conducted exclusively on male mice. While this choice was made to eliminate the confounding effects of cyclic hormonal variations on glycogen metabolism and to ensure data homogeneity during the initial discovery phase, it represents a significant limitation. Recent evidence underscores the pronounced sex differences in the epidemiology, metabolic signaling, and progression of MASLD/MASH [2]. Consequently, our findings regarding the glycogen structural signature may not fully encapsulate the pathophysiology in females. Future research incorporating female animal models and accounting for hormonal status is essential to substantiate the universal relevance of glycogen architecture as a therapeutic target.

Declaration of competing interest

The authors declare no competing financial interest.

References

[1] H. Tilg, S. Petta, N. Stefan, et al., Metabolic Dysfunction-Associated Steatotic Liver Disease in Adults: A Review, JAMA. 335 (2026) 163-174. https://doi.org/10.1001/jama.2025.19615.

[2] Y. Dai, Z. Lu, Y. Peng, et al., Serpina3c protects against metabolic dysfunction-associated steatotic liver disease in offspring induced by prenatal prednisone exposure, Signal Transduct Target Ther. 11 (2026) 71. https://doi.org/10.1038/s41392-025-02569-1.

[3] E. Guirguis, J. Dougherty, K. Thornby, et al., Resmetirom: The First Food and Drug Administration–Approved Medication for Nonalcoholic Steatohepatitis (NASH), Annals of Pharmacotherapy. 59 (2025) 162-173. https://doi.org/doi: 10.1177/10600280241259528.

[4] S.A. Harrison, P. Bedossa, C.D. Guy, et al., A Phase 3, Randomized, Controlled Trial of Resmetirom in NASH with Liver Fibrosis, New England Journal of Medicine. 390 (2024) 497-509. https://doi.org/10.1056/NEJMoa2309000.

[5] P. Drochmans, Morphologie du glycogene - etude au microscope electronique de colorations negatives du glycogene particulaire, J. Ultrastruct Res. 6 (1962) 141-163.

[6] X. Jiang, P. Zhang, S. Li, et al., The molecular-size dependence of glycogen enzymatic degradation rate and its importance for diabetes, Eur Polym J. 82 (2016) 175-180.

[7] Z. Hu, B. Deng, X. Tan, et al., Diurnal changes of glycogen molecular structure in healthy and diabetic mice, Carbohydr. Polym. 185 (2018) 145-152. https://doi.org/10.1016/j.carbpol.2018.01.003.

[8] B. Deng, M.A. Sullivan, A.C. Wu, et al., The mechanism for stopping chain and total-molecule growth in complex branched polymers, exemplified by glycogen, Biomacromolecules. 16 (2015) 1870-1872. http://pubs.acs.org/doi/pdfplus/10.1021/acs.biomac.5b00459

[9] Z. Wang, X. Min, Z. Hu, et al., The fragility of liver glycogen from humans with type 2 diabetes: A pilot study, Int.J.Biol Macromol. 221 (2022) 83-90. https://doi.org/https://doi.org/10.1016/j.ijbiomac.2022.08.212.

[10] Y. Chen, J. Zhu, J. Li, et al., O-GlcNAcylation increases PYGL activity by promoting phosphorylation, Glycobiology. 32 (2022) 101-109. https://doi.org/10.1093/glycob/cwab114.

[11] R.L. Koch, C. Soler-Alfonso, B.T. Kiely, et al., Diagnosis and management of glycogen storage disease type IV, including adult polyglucosan body disease: A clinical practice resource, Molecular Genetics and Metabolism. 138 (2023) 107525. https://doi.org/https://doi.org/10.1016/j.ymgme.2023.107525.

[12] X. Zhang, H. Yin, X. Zhang, et al., N6-methyladenosine modification governs liver glycogenesis by stabilizing the glycogen synthase 2 mRNA, Nature Communications. 13 (2022) 7038. https://doi.org/10.1038/s41467-022-34808-2.

[13] K. Uehara, W.D. Lee, M. Stefkovich, et al., mTORC1 controls murine postprandial hepatic glycogen synthesis via Ppp1r3b, The Journal of Clinical Investigation. 134 (2024) https://doi.org/10.1172/JCI173782.

[14] K.T. Creasy, M.B. Mehta, C.V. Schneider, et al., Ppp1r3b is a metabolic switch that shifts hepatic energy storage from lipid to glycogen, Science Advances. 11 (2025) eado3440. https://doi.org/10.1126/sciadv.ado3440.

[15] S.K. Bansal, M.B. Bansal, Pathogenesis of MASLD and MASH – role of insulin resistance and lipotoxicity, Alimentary Pharmacology & Therapeutics. 59 (2024) S10-S22. https://doi.org/https://doi.org/10.1111/apt.17930.

[16] S. Sabatini, P. Sen, F. Carli, et al., Hepatic glucose production rises with the histological severity of metabolic dysfunction-associated steatohepatitis, Cell Reports Medicine. 5 (2024) 101820. https://doi.org/https://doi.org/10.1016/j.xcrm.2024.101820.

[17] P. Cao, Y. Wang, C. Zhang, et al., Quercetin ameliorates nonalcoholic fatty liver disease (NAFLD) via the promotion of AMPK-mediated hepatic mitophagy, The Journal of Nutritional Biochemistry. 120 (2023) 109414. https://doi.org/https://doi.org/10.1016/j.jnutbio.2023.109414.

[18] P. Cao, M. Yue, Y. Cheng, et al., Naringenin prevents non-alcoholic steatohepatitis by modulating the host metabolome and intestinal microbiome in MCD diet-fed mice, Food Science & Nutrition. 11 (2023) 7826-7840. https://doi.org/https://doi.org/10.1002/fsn3.3700.

[19] W. Guo, L. Luo, Y. Meng, et al., Luteolin alleviates methionine–choline-deficient diet-induced non-alcoholic steatohepatitis by modulating host serum metabolome and gut microbiome, Frontiers in Nutrition. 9 (2022) 936237. https://doi.org/10.3389/fnut.2022.936237.

[20] M.G. O'Shea, M.S. Samuel, C.M. Konik, et al., Fluorophore-assisted carbohydrate electrophoresis (FACE) of oligosaccharides - efficiency of labelling and high-resolution separation, Carbohydr. Res. 307 (1998) 1-12.

[21] A.C. Wu, E. Li, R.G. Gilbert, Exploring extraction/dissolution procedures for analysis of starch chain-length distributions, Carbohydr. Polym. 114 (2014) 36-42. https://doi.org/10.1016/j.carbpol.2014.08.001.

[22] M.A. Sullivan, P.O. Powell, T. Witt, et al., Improving size-exclusion chromatography for glycogen, J. Chromatogr. A. 1332 (2014) 21-29.

[23] F. Vilaplana, R.G. Gilbert, Characterization of branched polysaccharides using multiple-detection size separation techniques, J. Sep. Sci. 33 (2010) 3537–3554. https://doi.org/10.1002/jssc.201000525.

[24] P.O. Powell, M.A. Sullivan, J.J. Sheehy, et al., Acid Hydrolysis and Molecular Density of Phytoglycogen and Liver Glycogen Helps Understand the Bonding in Glycogen α (Composite) Particles, PLoS One. 10 (2015) e0121337. https://doi.org/10.1371/journal.pone.0121337.

[25] P. Cao, Y. Zhang, Z. Huang, et al., The preventative effects of procyanidin on binge ethanol-Induced lipid accumulation and ROS overproduction via the promotion of hepatic autophagy, Molecular Nutrition & Food Research. 63 (2019) 1801255. https://doi.org/https://doi.org/10.1002/mnfr.201801255.

[26] Z. Hu, E. Li, M.A. Sullivan, et al., Glycogen structure in type 1 diabetic mice: towards understanding the origin of diabetic glycogen molecular fragility, Int.J.Biol Macromol. 128 (2019) 665-672.

[27] D. Jahn, S. Kircher, H.M. Hermanns, et al., Animal models of NAFLD from a hepatologist's point of view, Biochimica et Biophysica Acta (BBA) - Molecular Basis of Disease. 1865 (2019) 943-953. https://doi.org/https://doi.org/10.1016/j.bbadis.2018.06.023.

[28] X.S. Cui, H.Z. Li, L. Li, et al., Rodent model of metabolic dysfunction-associated fatty liver disease: a systematic review, J Gastroenterol Hepatol. 40 (2025) 48-66. https://doi.org/10.1111/jgh.16749.

[29] G.R. Romualdo, L.C. Valente, G.P. Bacil, et al., A diet-driven metabolic dysfunction-associated steatohepatitis (MASH) mouse model resembles the corresponding human disease, J Mol Histol. 56 (2025) 162. https://doi.org/10.1007/s10735-025-10449-9.

[30] M. Khoury, Q. Guo, K. Furuta, et al., Glycogen synthase kinase 3 activity enhances liver inflammation in MASH, JHEP Rep. 6 (2024) 101073. https://doi.org/10.1016/j.jhepr.2024.101073.

[31] E. Scoditti, S. Sabatini, F. Carli, et al., Hepatic glucose metabolism in the steatotic liver, Nat Rev Gastroenterol Hepatol. 21 (2024) 319-334. https://doi.org/10.1038/s41575-023-00888-8.

[32] C. Ma, S. Wang, B. Dong, et al., Metabolic reprogramming of immune cells in MASH, Hepatology. (2025) https://doi.org/10.1097/HEP.0000000000001371.

[33] H.-Z. Ying, Y.-H. Liu, B. Yu, et al., Dietary quercetin ameliorates nonalcoholic steatohepatitis induced by a high-fat diet in gerbils, Food and Chemical Toxicology. 52 (2013) 53-60. https://doi.org/https://doi.org/10.1016/j.fct.2012.10.030.

[34] Y.Q. Hua, Y. Zeng, J. Xu, et al., Naringenin alleviates nonalcoholic steatohepatitis in middle-aged Apoe−/−mice: role of SIRT1, Phytomedicine. 81 (2021) 153412. https://doi.org/https://doi.org/10.1016/j.phymed.2020.153412.

[35] G.R. Steinberg, D.G. Hardie, New insights into activation and function of the AMPK, Nature Reviews Molecular Cell Biology. 24 (2023) 255-272. https://doi.org/10.1038/s41580-022-00547-x.

[36] S. Yang, H. Duan, J. Zeng, et al., Luteolin modulates macrophage phenotypic switching via the AMPK-PPARγ pathway to alleviate ulcerative colitis in mice, Journal of Ethnopharmacology. 339 (2025) 119157. https://doi.org/https://doi.org/10.1016/j.jep.2024.119157.

[37] M. Zhu, Y. Sun, Y. Su, et al., Luteolin: A promising multifunctional natural flavonoid for human diseases, Phytotherapy Research. 38 (2024) 3417-3443. https://doi.org/https://doi.org/10.1002/ptr.8217.

[38] Y. Wang, X. Wang, Y. Qian, et al., Naringenin attenuates slow-transit constipation by regulating the AMPK/mTOR/ULK1 signaling pathway: In vivo and in vitro studies, The Journal of Nutritional Biochemistry. (2025) 110013. https://doi.org/https://doi.org/10.1016/j.jnutbio.2025.110013.

[39] A. Leszczynska, C. Stoess, H. Sung, et al., Extracellular Vesicles as Therapeutic and Diagnostic Tools for Chronic Liver Diseases, Biomedicines. 11 (2023) https://doi.org/10.3390/biomedicines11102808.

[40] L. Mao, W. Zhao, Y. Sun, et al., Diagnostic approaches optical imaging of GGT levels in lipid metabolism disorders: Insights from preclinical imaging and patients samples, Spectrochim Acta A Mol Biomol Spectrosc. 335 (2025) 125925. https://doi.org/10.1016/j.saa.2025.125925.